JOURNAL OF SPACECRAFT AND ROCKETS
Vol. 36, No. 6, November–December 1999

Multiple-Burn Families of Optimal Low- and Medium-Thrust Orbit Transfers

Jason C. H. Chuang*
Lockheed Martin Vought Systems Corporation, Dallas, Texas 75051
Troy D. Goodson†
Jet Propulsion Laboratory, California Institute of Technology, Pasadena, California 91109
and
John Hanson‡
NASA Marshall Space Flight Center, Huntsville, Alabama 35812

A new procedure for improving fuel- and time-optimal orbit transfers through burn additions is introduced and analyzed in terms of physical characteristics; results of its use are presented. The procedure is based on a property of the switching function for the optimal control problem. Criteria are given that may be used to determine whether other optimal control problems exhibit this property. This property and other properties of fuel-optimal orbit transfers related to number of burns and burn placement are examined. The orbit transfer problem formulation is given for final mass maximization allowing for second-harmonic oblateness effects, atmospheric drag effects, and three-dimensional, noncoplanar, nonaligned elliptic terminal orbits. A set of extremal solutions parameterized by transfer time, referred to as a family, are obtained using a combination of the new procedure, homotopy, and other numerical methods. Notably, this family exhibits multiplicity in solutions; that is, terminal orbits, transfer times, and numbers of burns are identically specified, but the resulting transfer trajectories and costs are different. Reasons are suggested why one transfer is favored over the other, using physical rationale. Effects of the drag and oblateness terms are discussed.

Nomenclature

C_D = craft's drag coefficient
C^i_j = space of functions with i continuous derivatives and j elements
$\boldsymbol{e}_T$ = thrust direction vector (unit vector)
e_x, e_y, e_z = Cartesian components of the eccentricity vector; additional subscript i or f indicates initial or final point, respectively
$\boldsymbol{F}_{\text{drag}}$ = force exerted by drag on the spacecraft
$\boldsymbol{F}_{\text{thrust}}$ = force exerted by the spacecraft's thruster on the spacecraft
$\boldsymbol{f}[\boldsymbol{x}(t), t]$ = that part of the differential equation for $\boldsymbol{x}(t)$ that does not vary with the control variables $u(t)$ and $\boldsymbol{v}(t)$
G = function, defined for convenience, that encompasses both the original performance index and the terminal constraints
g_0 = gravitational acceleration at sea level on Earth
$\boldsymbol{g}[\boldsymbol{x}(t), \boldsymbol{v}(t), t]$ = that part of the differential equation for $\boldsymbol{x}(t)$ that varies with the control variable $\boldsymbol{v}(t)$ and linearly with $u(t)$
H = Hamiltonian for the optimization problem; also $H[\boldsymbol{x}(t_f), T, \boldsymbol{e}_T(t_f), \boldsymbol{\lambda}(t_f)]$ or $H[\boldsymbol{x}(t), \boldsymbol{w}(t), u(t), \boldsymbol{\lambda}(t), t]$
H_T = switching function
h_x, h_y, h_z = Cartesian components of the angular momentum vector
I = identity matrix: diag{1, 1, 1}
I_{sp} = rocket motor specific impulse
J = performance index (to be maximized)
J_2 = constant describing the mass distribution of the central body
$L[\boldsymbol{x}(t), t]$ = used in theorem, function that entails the part of the performance index that does not vary with the control variable $u(t)$
$M[\boldsymbol{x}(t), t]$ = used in theorem, function that entails the part of the performance index that varies linearly with the control variable $u(t)$
$m(t)$ = spacecraft mass at time t
$\dot{m}$ = time rate of change of spacecraft mass, $m(t)$
m^* = reference mass, used for nondimensionalization
$\bar{N}$ = matrix: diag{1, 1, 3}
$Oxyz$ = Cartesian reference frame, centered at the attracting body
R = equatorial radius of the central body
r = magnitude of the spacecraft position vector
$\boldsymbol{r}(t)$ = radius vector, in Cartesian coordinates, from the center of the (fixed) gravitating body to the center of the spacecraft
r_0 = reference altitude for the atmospheric drag model
r^* = reference radius, used for nondimensionalization
S = wetted area of the craft
T = spacecraft thrust level
$T_{\max}$ = maximum spacecraft thrust level
t_f = length of time between the start and end of the transfer
U = gravitational potential
u, v, w = Cartesian components in $Oxyz$ of the velocity vector $\boldsymbol{v}$
v = speed or magnitude of the velocity vector
$\boldsymbol{v}$ = velocity vector with respect to the inertial reference frame
$\boldsymbol{w}(t)$ = used in theorem, continuous control
x, y, z = Cartesian components in $Oxyz$ of the position vector $\tilde{\boldsymbol{r}}$
$\boldsymbol{x}(t)$ = state vector, includes position, velocity, and mass, $[\boldsymbol{r}(t)^T \;\; \boldsymbol{v}(t)^T \;\; m(t)]^T$
β = air density variation in the prescribed altitude region

Received 4 March 1996; revision received 12 April 1999; accepted for publication 3 May 1999.
*Senior Staff Engineer, Guidance and Navigation.
†Engineer, Flight Path Control.
‡Team Leader, Trajectory and Guidance.

$\boldsymbol{\lambda}(t)$ = complete costate vector, $[\boldsymbol{\lambda}_r(t)^T \;\; \boldsymbol{\lambda}_v(t)^T \;\; \lambda_m(t)]^T$
$\boldsymbol{\lambda}_r(t)$ = $\tilde{\boldsymbol{r}}$ costate vector
$\boldsymbol{\lambda}_v(t)$ = $\tilde{\boldsymbol{v}}$ costate vector
μ = gravitational constant for the central body
ν_{f_j} = Lagrange multipliers on the boundary conditions
$\boldsymbol{\nu}$ = Lagrange multiplier vector corresponding to the boundary conditions, $[\boldsymbol{\nu}_{f_j}^T \;\; \boldsymbol{\nu}_{i_j}^T]^T$
ρ_0 = atmosphere density at the altitude r_0
υ = independent variable representing nondimensionalized time
$\psi(\boldsymbol{x})$ = terminal condition function, specifies terminal orbits
ψ_{i_1}–ψ_{i_5} = terminal conditions 1–5, where i indicates initial state, f indicates final state
$\hat{\ }$ = nondimensional quantity

Introduction

THE minimum fuel orbit transfer optimization problem has been studied for many years now. Some of the most complete early work[1] considering impulsive transfers presented an exact solution to the costate differential equations on a coasting arc. The optimality of the Hohmann transfer using early optimal control theory was also verified. In the finite-thrust arena, many recent papers have been written, some with direct and some with indirect methods. For example, using collocation once then direct transcription later, Enright and Conway[2,3] examined circular, point-to-point planar transfers with ideal gravity. Herein, ideal gravity refers to spherical body gravity, namely, a simple inverse-square law. Zondervan et al.[4] used a hybrid direct/indirect method to study three-burn point-to-point transfers with plane changes in ideal gravity and thrust levels down to a thrust-to-initial-weight ratio of 0.04. Vulpetti and Montreali[5] used nonlinear programming to optimize point-to-point transfers between circular orbits with inclinations. They included oblateness and drag effects, but did not study the effects of these terms in their model.

Among the studies using indirect methods, the work by Redding[6] handled point-to-point low-thrust transfers with plane changes. The study was limited to transfers to geosynchronous orbits in an ideal gravity field. Another indirect method[7] was actually a combination of two approaches. The first approximated ideal gravity using a model for gravitational accelerations linearly varying with altitude. This assumption results in a linear steering law and was used to simplify low-accuracy calculation of the transfer. The data from this approach were used as the starting iterate of another, more accurate code. Horsewood et al.[8] modified earlier work[9] (a minimum time formulation using equinoctial orbital elements) to produce a code for the optimization of point-to-point orbit transfers with plane changes between circular orbits with relatively low thrust in an ideal gravity field. Brown et al.[10] produced an indirect method, named OPGUID/SWITCH, which handles free entry/exit points and free final time using a reduced set of boundary conditions. Redding[6] formulated the problem with transfer-time optimization as did Brown et al.,[10] whereas Horsewood et al.[8] fixed the final time.

This paper complements these studies by considering a formulation that sets free the entry/exit points and the final time for optimization and includes realistic effects such as oblateness and drag for the study of optimal transfer. The questions of optimizing the final time and of optimizing the entry/exit points are investigated. A new method for increasing the number of burns a transfer executes is presented.

The performance index is defined simply as the final mass of the spacecraft including fuel; this quantity will be maximized. The equations of motion are stated in terms of the gravity model with oblateness effects and an assumed atmosphere model for drag.

The Hamiltonian is linear with respect to the thrust (control). This linearity results in bang-bang control or singular arc solutions for the maximization problem. Although bang-bang control is assumed here, the possibility of having a singular arc has not been ruled out for a general case. To determine whether a singular arc solution would occur, the derivative of the switching function at each switching point is checked; switching points are defined herein as points where the switching function vanishes, for example, points where the bang-bang control switches from one extreme to the other. If the iterative routines obtain a nonoptimal solution, high-frequency chattering in thrust may occur within the numerical accuracy of the routines. This chattering may indicate that singular-arc solutions are possible for some modification of system parameters and models. However, for the solutions presented in this paper, no high-frequency chattering occur.

Numerical solutions to specific optimal transfer problems are presented. These solutions represent the ability of two-point boundary-value-problem (TPBVP) solvers. The solvers used were BOUNDSCO, a multipoint shooting algorithm,[11] and the minimizing boundary-condition method (MBCM),[12] a modification to the shooting method.

Consider the free transfer-time optimal control problem and the idea of improving fuel savings by adding burns. For impulsive thrust between circular orbits, the Hohmann transfer gives minimum fuel use. The three-impulse bielliptic transfer performs better than the two-impulse Hohmann transfer for radius ratios greater than 11.939 (Ref. 13). Additionally, Lion and Handelsman[14] have done excellent work in using primer vector theory to determine ways of improving impulsive trajectories. To our knowledge, similar conclusions for low- and medium-thrust transfers have not been shown anywhere. One hypothesis is that the global extremum will be at infinite transfer time and that local extremum solutions exist for finite transfer times. Furthermore, for a given number of burns there may be a local extremum with finite transfer time. Suppose one has obtained such a local extremal: Is there an easy way to add a burn and improve this trajectory? Are there any pitfalls to be aware of? What if the solution takes into account atmospheric drag and oblateness effects? This paper attempts to answer these questions using solutions obtained by the methods just mentioned.

Problem Formulation

The problem discussed is the following: Maximize the final mass of a thrusting spacecraft for an orbital transfer between two given terminal orbits without specifying the initial burn-on point, the final burn-off point, or the overall transfer time. Therefore, the performance index can be written as

$$J = m(t_f) \tag{1}$$

The spacecraft is represented by a point mass and assumed to be a thrusting craft acted upon by aerodynamic drag and oblate-body gravity forces of a central body. Thrust is written as a time-varying magnitude T independent of a time-varying direction $\boldsymbol{e}_T$:

$$\boldsymbol{F}_{\text{thrust}} = T\boldsymbol{e}_T \tag{2}$$

For a three-dimensional thrust vector the control in Eq. (2) requires a magnitude T and three components in $\boldsymbol{e}_T$ or two angles. For two-dimensional problems, one magnitude and two components in $\boldsymbol{e}_T$ or one angle are required. The mass will decrease according to

$$\dot{m} = -\frac{T}{g_0 I_{\text{sp}}} \tag{3}$$

The atmosphere surrounding the central body is described with an exponential model. The following equation[15] describes such a drag force:

$$\boldsymbol{F}_{\text{drag}} = -\tfrac{1}{2}\rho_0 e^{-\beta(r-r_0)} SC_D v\boldsymbol{v} \tag{4}$$

It is assumed that the product SC_D is not a function of time and that the craft always remains in a region where the chosen exponential atmosphere model is valid.

Within the confines of this study, the only other influence on the craft is gravitational potential energy. The gravitational potential energy to the second harmonic[16] is

$$U = -\left(\frac{\mu m}{r}\right) - \left[\frac{\mu J_2 R^2 m}{2r^3}\right]\left[1 - 3\left(\frac{z}{r}\right)^2\right] \tag{5}$$

There are additional mass distribution terms, but the series is truncated here. The equations of motion can be determined by evaluating $-\partial U/\partial \boldsymbol{r}$ and by using Eqs. (2) and (4). The equations of motion, written as a first-order system in vector–matrix form, are

$$\dot{\boldsymbol{r}} = \boldsymbol{v} \tag{6a}$$

$$\dot{\boldsymbol{v}} = \left(\frac{T}{m}\right)\boldsymbol{e}_T - \left(\frac{\mu}{r^3}\right)\boldsymbol{r} - \left\{\frac{3\mu J_2 R^2}{2r^5}\left[\bar{N} - 5\left(\frac{z}{r}\right)^2 I\right]\right\}\boldsymbol{r} - \left[\rho_0 e^{-\beta(r-r_0)}\frac{SC_D}{(2m)}\right]v\boldsymbol{v} \tag{6b}$$

$$\dot{m} = -\frac{T}{g_0 I_{\mathrm{sp}}} \tag{6c}$$

where $\bar{N} = \mathrm{diag}\{1, 1, 3\}$ (where diag denotes a matrix whose elements are zero except for the diagonals and whose elements are specified in the braces) and I is the identity matrix.

The thrust magnitude has both an upper and a lower bound. The upper bound is $T_{\max}$, the lower bound is zero. Therefore, an inequality constraint that must be satisfied for all time $t \in [0, t_f]$ is

$$0 \le T \le T_{\max} \tag{7}$$

Finally, the terminal orbits are specified by the vector equations

$$\psi_i[\boldsymbol{x}(0)] = 0 \tag{8a}$$

$$\psi_f[\boldsymbol{x}(t_f)] = 0 \tag{8b}$$

that are only satisfied when the initial and final states both lie on their respective prescribed orbits. These conditions do not fix the initial and final states; they fix all of the orbital elements except position on the orbit, that is, true anomaly. Consequently, for three-dimensional problems the vector function $\psi(\boldsymbol{x})$ has five components, not six. In this paper,

$$\psi_{i_1} = yw - zv - h_{x_i} \tag{9a}$$

$$\psi_{i_2} = zu - xw - h_{y_i} \tag{9b}$$

$$\psi_{i_3} = xv - yu - h_{z_i} \tag{9c}$$

$$\psi_{i_4} = [(v^2 - \mu/r)x - (\boldsymbol{r}^T\boldsymbol{v})u] - \mu e_{x_i} = 0 \tag{9d}$$

$$\psi_{i_5} = [(v^2 - \mu/r)y - (\boldsymbol{r}^T\boldsymbol{v})v] - \mu e_{y_i} = 0 \tag{9e}$$

These equations are written for the initial orbit. The equations for the final orbit are identical except that the subscript i is replaced with f.

All that is required is the angular momentum and eccentricity vectors. In the full three-dimensional case, the number of components of these two vectors sums to 12 (6 from each orbit). However, because the angular momentum and the eccentricity vectors are perpendicular, one component will be redundant and thus removable. For Eqs. (9a–9e) the z component of the eccentricity vector has been removed. This choice anticipates that transfers examined occur in or near the x–y plane. In the two-dimensional case the angular momentum vector has two zero components, whereas the eccentricity vector has one zero component.

In the two-dimensional case, it would seem that the ellipse equation and the energy equation could be used in place of the eccentricity vector constraint [Eqs. (9d) and (9e)]. However, the combined specification of orbit geometry, energy, and angular momentum does not uniquely determine an orbit. Angular momentum and energy do determine the semimajor axis and the eccentricity. However, the ellipse may be rotated to find more than one argument of perigee such that the specified conic section is intersected and the proper velocity magnitude, but not direction, is matched. The reason for this possibility is the existence of two different velocity vectors at one point in space with the same angular momentum and energy.

First-Order Necessary Conditions

The Hamiltonian function specific for the problem is

$$H = \boldsymbol{\lambda}_{\mathrm{r}}^T\boldsymbol{v} + \boldsymbol{\lambda}_v^T\left\{\left(\frac{T}{m}\right)\boldsymbol{e}_T - \left(\frac{\mu}{r^3}\right)\boldsymbol{r} - \left[\frac{3\mu J_2 R^2}{2r^5}\right] \times \left[\bar{N} - 5\left(\frac{z}{r}\right)^2 I\right]\boldsymbol{r} - \frac{1}{2}\left(\frac{\rho_0}{m}\right)e^{-\beta(r-r_0)}SC_D v\boldsymbol{v}\right\} - \frac{\lambda_m T}{g_0 I_{\mathrm{sp}}} \tag{10}$$

Consistent with Lawden's primer vector theory,[1] it is found that for $T = 0$

$$\boldsymbol{e}_T = \boldsymbol{\lambda}_v/|\boldsymbol{\lambda}_v| \tag{11}$$

The optimal thrust magnitude T is governed by the following switching function and switching condition:

$$H_T = \frac{\partial H}{\partial T} = \boldsymbol{\lambda}_v^T\frac{\boldsymbol{e}_T}{m - \lambda_m}\Big/(g_0 I_{\mathrm{sp}}) = \frac{|\boldsymbol{\lambda}_v|}{m - \lambda_m}\Big/(g_0 I_{\mathrm{sp}}) \tag{12}$$

$$H_T > 0, \qquad T = T_{\max}, \qquad H_T < 0, \qquad T = 0 \tag{13}$$

This relationship between the bang-bang control and the switching function, referred to as the switching structure, satisfies the Pontryagin maximum principle by maximizing the Hamiltonian using T. If H_T were to be zero for a finite time the control would be singular. Higher-order derivatives of H_T would then be needed to calculate T.

The costate dynamics can be found from the following Euler–Lagrange equations:

$$\dot{\boldsymbol{\lambda}}_{\boldsymbol{r}} = \mu\left[\frac{\boldsymbol{\lambda}_v}{r^3} - \frac{3\left(\boldsymbol{\lambda}_v^T\boldsymbol{r}\right)\boldsymbol{r}}{r^5}\right] - \left[\frac{\rho_0\beta}{2m}\right]e^{-\beta(r-r_0)}SC_D v\left(\boldsymbol{\lambda}_v^T\boldsymbol{v}\right)\left(\frac{\boldsymbol{r}}{r}\right) + \frac{3}{2}\mu J_2 R^2\left[\frac{\bar{N}\boldsymbol{\lambda}_v}{r^5} - \frac{5\left(\boldsymbol{\lambda}_v^T\bar{N}\boldsymbol{r}\right)\boldsymbol{r}}{r^7}\right] - \left(\frac{15}{2}\right)\mu J_2 R^2 \times \left\{\left(\frac{z^2}{r^7}\right)\boldsymbol{\lambda}_v - \left(\boldsymbol{\lambda}_v^T\boldsymbol{r}\right)\left[\left(\frac{7z^2}{r^9}\right)\boldsymbol{r} - \left(\frac{2z}{r^7}\right)\begin{bmatrix}0\\0\\1\end{bmatrix}\right]\right\} \tag{14}$$

$$\dot{\boldsymbol{\lambda}}_v = -\boldsymbol{\lambda}_r + \left[\frac{\rho_0}{(2m)}\right]e^{-\beta(r-r_0)}SC_D\left[\boldsymbol{\lambda}_v v + \frac{\left(\boldsymbol{\lambda}_v^T\boldsymbol{v}\right)\boldsymbol{v}}{v}\right] \tag{15}$$

$$\dot{\lambda}_m = \left(\frac{T}{m^2}\right)\boldsymbol{\lambda}_v^T\boldsymbol{e}_T - \left[\frac{\rho_0}{(2m^2)}\right]e^{-\beta(r-r_0)}SC_D v\boldsymbol{\lambda}_v^T\boldsymbol{v} \tag{16}$$

To complete the TPBVP, the methods of optimal control supply a set of natural boundary conditions

$$\boldsymbol{\lambda}(t_f) = \left[\frac{\partial G}{\partial \boldsymbol{x}(t_f)}\right]^T \tag{17a}$$

$$\boldsymbol{\lambda}(0) = -\left[\frac{\partial G}{\partial \boldsymbol{x}(0)}\right]^T \tag{17b}$$

where G is constructed for our problem as

$$G = m(t_f) + \left[\nu_{i_1}\psi_{i_1} + \nu_{i_2}\psi_{i_2} + \nu_{i_3}\psi_{i_3} + \nu_{i_4}\psi_{i_4} + \nu_{i_5}\psi_{i_5}\right] + \left[\nu_{f_1}\psi_{f_1} + \nu_{f_2}\psi_{f_2} + \nu_{f_3}\psi_{f_3} + \nu_{f_4}\psi_{f_4} + \nu_{f_5}\psi_{f_5}\right] \tag{18}$$

For $t = t_f$, the natural boundary conditions are

$$\lambda_x = -\nu_{f_2} w + \nu_{f_3} v + \nu_{f_4}(v^2 + w^2 - \mu/r + \mu x^2/r^3) + \nu_{f_5}(\mu xy/r^3 - uv) \tag{19a}$$

$$\lambda_y = \nu_{f_1} w - \nu_{f_3} u + \nu_{f_4}\frac{\mu xy}{r^3 - uv} + \nu_{f_5}\left(u^2 + w^2 - \frac{\mu}{r} + \frac{\mu y^2}{r^3}\right) \tag{19b}$$

$$\lambda_z = -\nu_{f_1} v + \nu_{f_2} u + \nu_{f_4}\frac{\mu xz}{r^3 - uw} + \nu_{f_5}\frac{\mu yz}{r^3 - vw} \tag{19c}$$

$$\lambda_u = \nu_{f_2} z - \nu_{f_3} y + \nu_{f_4}(-yv - zw) + \nu_{f_5}(2yu - xv) \tag{19d}$$

$$\lambda_v = -\nu_{f_1} z + \nu_{f_3} x + \nu_{f_4}(2xv - uy) + \nu_{f_5}(-xu - zw) \tag{19e}$$

$$\lambda_w = \nu_{f_1} y - \nu_{f_2} x + \nu_{f_4}(2xw - uz) + \nu_{f_5}(2yw - vz) \tag{19f}$$

$$\lambda_m = 1 \tag{19g}$$

The natural boundary conditions at $t = 0$ are identical to Eqs. (19a–19f) but with a negative sign placed in front of the right-hand side of the equations as indicated by Eq. (17b) and ν_f replaced by ν_i.

The last condition deals with the final time. For free transfer-time problems, the transversality condition must be satisfied:

$$H[\boldsymbol{x}(t_f), T, \boldsymbol{e}_T(t_f), \lambda(t_f)] = \frac{-\partial G}{\partial t_f} = 0 \tag{19h}$$

However, in some solutions presented the transfer time is fixed. By looking at the characteristics of the solutions as the transfer time is varied toward the optimal value, we may gain some important insights into the nature of this optimization.

New Property of the Optimal Switching Function

A very interesting property of the solution with optimal transfer time is that not only are the initial and final values of the switching function equal, but they are both equal to zero.

This property may be explained with the following theorem. In what follows, C_j^i refers to the space of i-dimensional function functions with j continuous derivatives.

Theorem 1: Given a bang-bang optimal control problem of the form

$$J = \int_{t_i}^{t_f} [L(\boldsymbol{x}(t), t) + M(\boldsymbol{x}(t), t)u(t)]\,\mathrm{d}t$$

where functions L and M are continuous and subject to the following:

$$\dot{\boldsymbol{x}}(t) = \boldsymbol{f}[\boldsymbol{x}(t), t] + \boldsymbol{g}[\boldsymbol{x}(t), \boldsymbol{w}(t), t]u(t)$$

$$\boldsymbol{x}(t) \in C_0^n, \qquad \boldsymbol{w}(t) \in C_0^m$$

where $u_{\min} \le u(t) \le u_{\max}$ and $\boldsymbol{u}(t) \in \boldsymbol{U}$ is a piecewise continuous scalar control,

$$\psi_i[\boldsymbol{x}(t_i)] = 0, \qquad \psi_f[\boldsymbol{x}(t_f)] = 0$$

$$\psi_i[\boldsymbol{x}(t_i)] \in C_0^{q_1}, \qquad \psi_f[\boldsymbol{x}(t_f)] \in C_0^{q_2}$$

and where t_i and t_f are free for optimization. Satisfy the following assumptions:

1) Assume $L[\boldsymbol{x}(t_i), t_i) = L(\boldsymbol{x}(t_f), t_f)]$.

2) Assume $[\partial\psi_i(\boldsymbol{x}(t))/\partial\boldsymbol{x}(t)]\boldsymbol{f}(\boldsymbol{x}(t), t) = 0$ and $[\partial\psi_f(\boldsymbol{x}(t))/\partial\boldsymbol{x}(t)]\boldsymbol{f}(\boldsymbol{x}(t), t) = 0$.

3) Assume $u(t_i) = u(t_f) \neq 0$.

Then, considering the usual optimal control formulation, that is, introduction of the $\boldsymbol{\lambda}(t)$ functions and the Hamiltonian $H[\boldsymbol{x}(t), \boldsymbol{w}(t), u(t), \boldsymbol{\lambda}(t), t]$ function,[17] the following statements are true:

1) The switching function, $H_T[\boldsymbol{x}(t), \boldsymbol{\lambda}(t), t] = \boldsymbol{\lambda}(t)^T\boldsymbol{g}[\boldsymbol{x}(t), \boldsymbol{w}(t), t] + M[\boldsymbol{x}(t), t]$, satisfies $H_T[\boldsymbol{x}(t_i), \boldsymbol{\lambda}(t_i), t_i] = H_T[\boldsymbol{x}(t_f), \boldsymbol{\lambda}(t_f), t_f] = -L[\boldsymbol{x}(t_f), t_f]/u(t_f)$ if and only if $H[\boldsymbol{x}(t_i), \boldsymbol{w}(t_i), u(t_i), \boldsymbol{\lambda}(t_i), t_i] = 0$ and $H[\boldsymbol{x}(t_f), \boldsymbol{w}(t_f), u(t_f), \boldsymbol{\lambda}(t_f), t_f] = 0$.

2) If the Hamiltonian is autonomous with t_i and t_f fixed, then $H_T[\boldsymbol{x}(t_i), \boldsymbol{\lambda}(t_i)] = H_T[\boldsymbol{x}(t_f), \boldsymbol{\lambda}(t_f)]$ and $H_T[\boldsymbol{x}(t_f), \boldsymbol{\lambda}(t_f)] = [H(\boldsymbol{x}(t_f), \boldsymbol{w}(t_f), u(t_f), \boldsymbol{\lambda}(t_f)) - L(\boldsymbol{x}(t_f), t_f)]/u(t_f)$.

This theorem applies to any optimal control problem with a scalar bang-bang control and boundary conditions that involve only constants of motion. In other words, the boundary conditions cannot be functions of time, even implicitly, for unforced motion; this is the basis of assumption 2. The theorem is useful because it leads to a method for finding time-optimal extremals with additional $u_{\max}$ arcs when $u_{\min} = 0$. Although not attempted in this work, it may also lead to a method for finding extremals with fewer $u_{\max}$ arcs.

Applied to the orbit transfer problem with ideal gravity and free transfer time, the assumptions are clearly satisfied. Assumption 1 is satisfied because the L function is zero. Assumption 2 is satisfied because the boundary conditions are the orbital elements and the unforced dynamics assume ideal gravity. Assumption 3 simply specifies that the only interesting solutions are those that begin with the thrust turning on and end with the thrust turning off. Therefore, condition 1 implies the switching function must be zero at the entry/exit points. A similar condition was successfully used in the place of Eqs. (19a–19f) by Brown et al.[10] for free transfer-time problems in ideal gravity; however, that analysis was not extended to the constrained transfer-time case nor expressed for the more general class of optimal control problems. An example of condition 2 will be seen later.

Considerations for Numerical Solutions

The differential equations (6a–6c) and Eqs. (14–16) are written with respect to the independent variable t (time). Because neither numerical method used is written to iterate on the transfer time, this variable needs to be part of the algorithm's unknowns. The following scaling is made:

$$t = t_f \upsilon \tag{20}$$

where υ is the new independent variable, nondimensional time, to be used in the place of t. Therefore, to implement this scaling, t_f must multiply the derivatives of the states and costates and $\upsilon \in [0, 1]$.

Any atmosphere is usable by simple substitution early in the derivation of the differential constraint. For the purposes of this paper, a simple atmosphere model was chosen. The model is not intended to accurately represent the Earth's atmosphere, or any other planet. It is implemented only for the purpose of demonstrating the methods used and to allow examination of its effects on the optimal transfer.

The model is defined from a reference altitude of 450 km above the planet's equator. The entire atmosphere region is assumed isothermal with a temperature of 1000 K. The density at the definition altitude is 1.184×10^{-12} kg/m^3. The definition point for this model was taken from the 1976 U.S. Standard Atmosphere.[18]

The problem has been nondimensionalized. The nondimensionalization aids in a few ways. First, the integration of the state is more accurate because all variations are on the same order. Second, convergence is improved because all of the boundary conditions are immediately placed at or near the same order. The nondimensionalizations follow:

$$\hat{t}_f \equiv t_f \Big/ \sqrt{r^{*3}/\mu} \tag{21a}$$

$$\hat{\boldsymbol{v}} \equiv \boldsymbol{v}/\sqrt{\mu/r^*} \tag{21b}$$

$$\hat{\boldsymbol{r}} \equiv \boldsymbol{r}/r^* \tag{21c}$$

$$\hat{m} \equiv m/m^* \tag{21d}$$

and they require the following:

$$\hat{r}_0 \equiv r_0/r^* \tag{21e}$$

$$\hat{\beta} \equiv \beta r^* \tag{21f}$$

$$(\hat{\rho}_0 \hat{S} \hat{C}_D) \equiv \rho_0 S C_D (r^*/m^*) \tag{21g}$$

$$(\hat{g}_0 \hat{I}_{sp}) \equiv g_0 I_{sp} \sqrt{r^*/\mu} \tag{21h}$$

$$\hat{T} \equiv (T/m^*) \Big/ \left(\mu / r^{*2}\right) \tag{21i}$$

$$\hat{R}_0 \equiv R_0/r^* \tag{21j}$$

The choices of r^* and m^* are completely arbitrary. However, after a problem is solved by these nondimensionalizations, rescaling must be exercised with caution. If the rescaling is not consistent with the atmosphere model, the results are invalid; for example, rescaling also rescales the atmosphere model [note Eq. (4) and Eqs. (21e–21j)].

It can be shown that the nondimensional dynamic equations are equivalent to the dimensional dynamic equations with $\mu = 1$ (the value of J_2, however, has no dimensions and is not changed).

Numerical Methods

One method used here to solve the TPBVP is the multiple-point shooting method. The specific FORTRAN routines are those of BOUNDSCO.[11]

The state defined for the optimal control problem differs slightly from the state used by BOUNDSCO. The state used by BOUNDSCO includes the ν vector, from the natural boundary conditions in Eqs. (19a–19f), at both the initial and final times. This inclusion requires also that the system dynamics includes a corresponding number of zero derivatives; that is, ν does not vary with time. Another approach would be to solve a system of all but one of the natural boundary conditions for ν and substitute the result into the remaining equation, using it in place of the others. Still another approach would be to use the result of Theorem 1 as an equivalent condition. This may seem desirable, one equation in the place of several; however, the simple structure of the several equations seems to be much more tractable for BOUNDSCO than the complex structure of the one equation. BOUNDSCO does not allow switching structures that depend on the sign (polarity) of the switching function, but only on its zeros, or switching times. These switching times are iterated upon to compute a solution. The guessing of these switching times requires a brief explanation. In the free exit/entry point formulation, a coast arc of any duration may be appended before the initial burn-on point (or after the final burn-off point) without altering the optimality of the transfer. It then makes no sense to construct a solution with an initial coast arc because the first point in the initial guess would be indeterminate. Therefore, one can always assume switching structures that begin with a thrusting arc and that end with a thrusting arc.

The user guesses the switching points and specifies the switching conditions. Through iteration, BOUNDSCO attempts to make the state and time at a switching point satisfy the switching condition. Until such a match is made, BOUNDSCO uses the current best estimate of the switching times to indicate when the thrust is on or off. BOUNDSCO does not introduce nor remove switching points.

The second method used is MBCM.[12] This method is a modification of the simple shooting method. It expands the set of available solutions by removing one boundary condition while keeping the same number of unknowns. The choice of this boundary condition is arbitrary. Because there is one less boundary condition than unknown, the set of solutions become a one-dimensional family. With a larger set of solutions, it should be much easier to solve the resulting boundary-value problem. The search for the solution that incorporates the final boundary conditions is treated as a minimization problem. The square of one boundary condition is minimized while the others are kept as constraints. A sequential programming algorithm is used to solve the problem. The gradient is numerically calculated and used to update the initial state until the last boundary condition is satisfied. This method is at least as effective as BOUNDSCO in solving the TPBVPs for the current solved optimal orbit transfers.

The switching structure of the optimal control is implicit in MBCM. The program checks the switching function at each integration step. If the switching function alters sign at one integration step, the program stops the integration. A secant method then iterates to find the switching function's zero point. From our experience with MBCM, some sensitive problems need 14 digits of accuracy in their switching function. Once the integration passes the switching points, the program changes the thrust level according to the switching condition and returns to the normal step size for integration.

Optimal Entry/Exit Points

It is often more difficult to solve the free terminal-points problem than the rendezvous problem, namely, fixed terminal points. In this section a simple homotopy approach for determining the optimal terminal points is described, beginning with a solution to the fixed transfer-time rendezvous problem.

With such a solution, one way of determining the optimal choice of the final point is to simply obtain a set of solutions with varying final points but fixed transfer time and a fixed initial point. Compare the resulting final mass values. Choose the value corresponding to the maximum. Use this solution as a guess for the free final-point problem. Repeat the process, this time varying the initial point. These terminal point choices should be good guesses for the free terminal-point solution.

Figure 1 shows the last step of the approach: the free final-point problem has been solved, and solutions to this problem have been obtained for various initial rendezvous points. The results are quite satisfactory. There is one obvious local maximum in the range of values searched. This point approximates the best initial point.

Optimal Transfer Time

Before exploring the addition of burns, the only parameter that remains to be freed is the transfer time. An approach exactly analogous to that used in the preceding section is easily imagined for finding the optimal transfer time. Figure 2 shows cost associated with solutions over a range of final times. No solution represented in Fig. 2 has more than two burns. In obtaining these solutions a few interesting properties were noticed: 1) As the transfer time was lowered, the coasting arc was shortened; in fact, at the shortest transfer time examined, there was effectively no coasting arc. 2) For every solution in this set, the initial and final values of the switching function are equal, as predicted by Theorem 1. 3) As the transfer time was increased, no extremal solution was found beyond a certain transfer time, and the cost for this transfer time appeared to be locally maximized with respect to transfer time. The Hamiltonian function was found approximately equal to zero for these solutions.

The lower bound makes perfect intuitive sense: This is the quickest that one can do the transfer in an optimal fashion. It is also the least fuel efficient because the motor is on for the entire transfer.

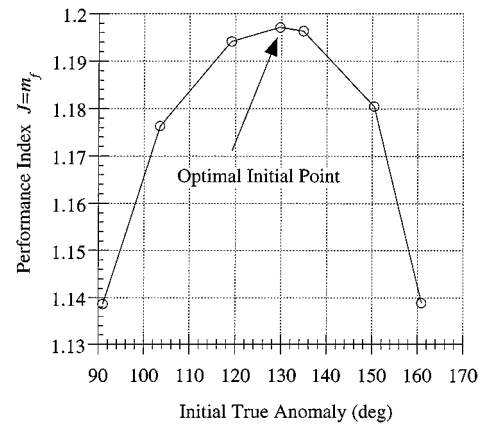

Fig. 1 Performance index vs true anomaly of initial orbit exit point.

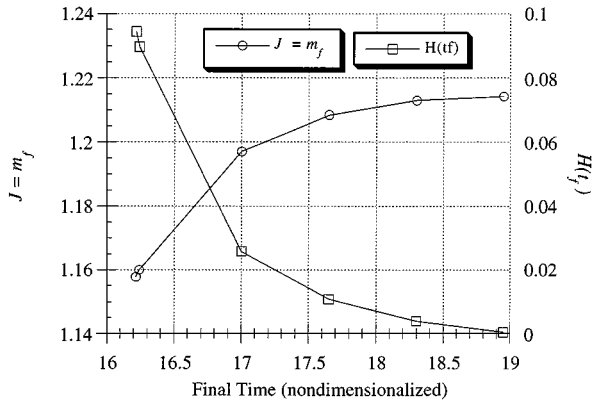

Fig. 2 Performance index and Hamiltonian vs final time for successive solutions.

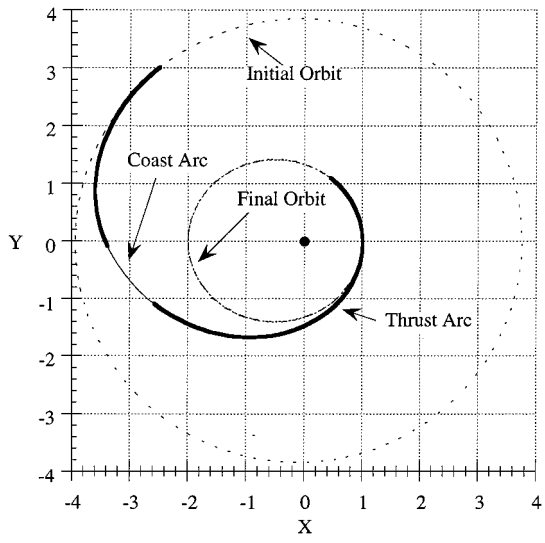

Fig. 3 Two-burn example transfer (nondimensional coordinates).

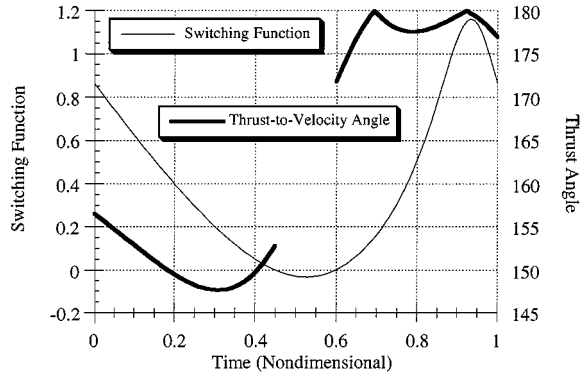

Fig. 4 Thrust-to-velocity angle and switching function for two-burn transfer (Fig. 3).

As for a so-called upper bound, not much can be said because not finding a solution does not mean a solution does not exist. However, taking the solution with the greatest transfer time found as a guess, the transversality condition was converged. It can be seen in Fig. 2 that for solutions progressing toward the optimal transfer time the Hamiltonian does, in fact, go to zero. As predicted by Theorem 1, the switching function values also go to zero.

Two-Burn Extremal

A particular solution is presented in this section, obtained by both methods. It has been nondimensionalized and performs in ideal gravity. The transfer is made between two planar, aligned orbits.

The solution's trajectory is shown in Fig. 3, and a plot of the thrust vector angle is shown in Fig. 4 superimposed upon the switching function. It corresponds to a trajectory represented by a point at $\hat{t}_f = 17$(4 h) in Fig. 2. The initial semimajor axis is 3.847 (roughly 25,305 km), and eccentricity is 0.02378. The final orbit semimajor axis is 1.5 (9867 km) and eccentricity is 0.333. The product $\hat{g}_0 \hat{I}_{sp}$ is 1.313 (an I_{sp} of 1043 s) and the thrust level is 0.03 (about 83 N). The initial mass is 1.527 (458 kg), and the final mass is 1.197 (359 kg).

Two burns are used to complete the transfer. For the first burn, $\Delta t = 108$ min and imparts a change in energy, $\Delta E = -3.82$ km^2/s^2, and in angular momentum, $\Delta h = -28{,}562$ km^2/s. For the coast, $\Delta t = 36$ min on an orbit of $a = 17{,}037$ km, $e = 0.4897$, and $\omega = -29.85$ deg. For the second burn $\Delta t = 96$ min and imparts an energy change, $\Delta E = -8.50$ km^2/s^2, and a change in angular momentum, $\Delta h = -12{,}719$ km^2/s. Most of the change in energy occurs in the longer second burn, but most of the change in angular momentum occurs in the first burn.

Figure 4 shows the switching function and the angle between the thrust vector and the velocity vector as functions of nondimensional time. Note that all thrusting during the transfer is roughly retrograde and, as predicted by Theorem 1, the initial and final values of the switching function are equal.

Family of Extremals via a New Method

Exploitation of the property described earlier using Theorem 1, along with the favorable performance of these indirect methods, has allowed the study of the characteristics of families of solutions. Herein a family of solutions is a set of solutions whose transfer times and numbers or burns vary but whose terminal orbits do not. The optimal terminal points will vary from solution to solution; they are free for optimization.

Figure 5 shows a family of optimal transfers. Each data point in Fig. 5 represents an extremal orbit transfer by its total transfer time and final mass. Each of these extremals satisfy the necessary conditions for maximizing the final mass and free entry/exit points on the terminal orbits. Their terminal orbits are the same as for the transfer given earlier and shown in Fig. 3. The terminal orbits are equatorial orbits, and the dynamics do not take drag or oblateness effects into account.

Though this family appears quite disjointed, it is actually quite connected. These connections can be best seen by starting at the leftmost transfer (point 1 in Fig. 5) and tracing solutions of increasing transfer time. The solutions from point 1 to point 2 are a set of two-burn solutions. However, at point 1 the total burn time equals the transfer time; point 1 may also be considered a one-burn solution (the switching function and its slope are zero). Point 2 represents a local optima in transfer time; the Hamiltonian for point 2 is zero, and this satisfies the transversality condition.

The switching function at point 2 indicates the existence of additional solutions. The situation is shown in Fig. 6 (labeled "Original Transfer"). Because H_T is zero at both the initial and final times (from Theorem 1) and its slope is positive at the initial time and negative at the final time, the transfer may be extended optimally by the addition of a coast at the beginning and/or at the end of the transfer. This may seem trivial: One might observe that coast arcs can always be added; however, this particular situation leads to the addition of burns. Lawden's solution[1,19] to the costates on a coast arc shows that on such an arc with a zeroed Hamiltonian the switching function is periodic. This result means that the switching function, once crossing zero, must return to zero. In other words, for an n burn transfer such as that represented by Fig. 6, the periodicity of the coast arc switching function implies the possible existence of an $n + 1$ burn solution. Moreover, this periodicity indicates the possible existence of two different $n + 1$ burn solutions and an $n + 2$ burn solution. Note that, to optimally extend a transfer and add a burn, it is required that the switching function at a terminal orbit both be equal to zero and have an appropriate sign for its slope: positive at the initial time and/or negative at the final time.

Adding the coast arc is trivial; adding the burn arc is not. The following burn-addition procedure worked well: 1) Append a coast arc to the solution at the chosen time, initial or final time, making sure that states and costates are continuous. This procedure is easily done by integrating the state and costate forward from the final time

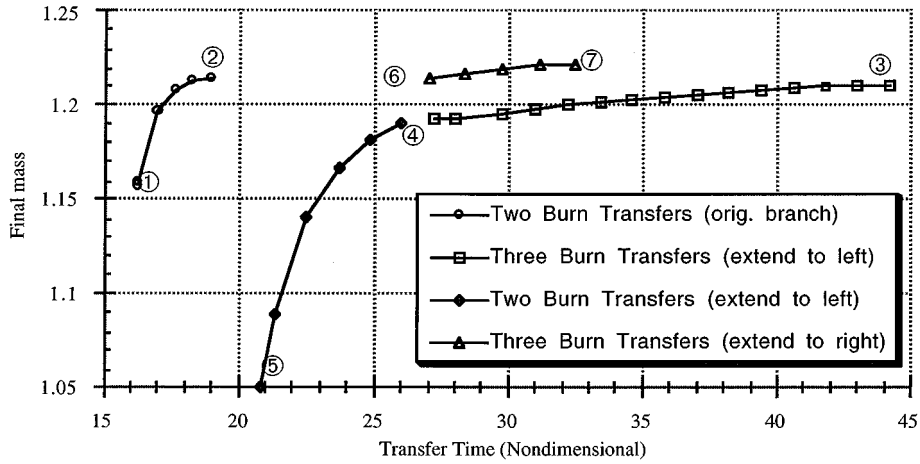

Fig. 5 Family of optimal transfers as final mass vs transfer time.

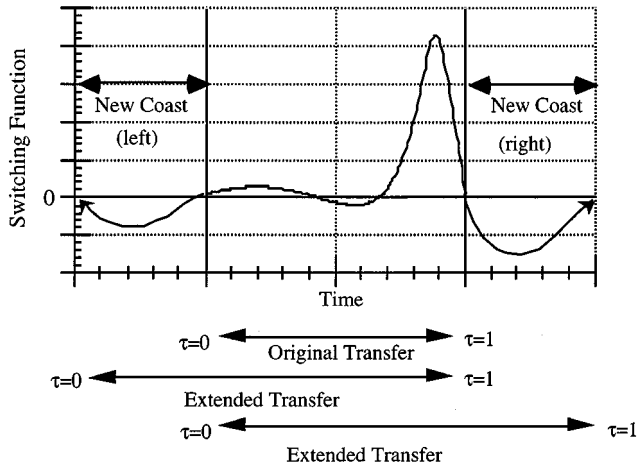

Fig. 6 Extending the switching function to create more optimal transfers.

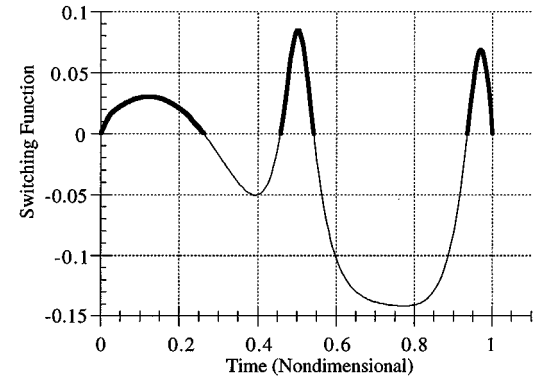

Fig. 7 Switching function of transfer at point 7 in Fig. 5.

or backward from the initial time. At both ends of the new coast arc, the switching function must be zero. 2) Use this extended transfer as a guess for the numerical routine assuming an $n + 1$ burn problem and a slightly longer transfer time. 3) Apply homotopy to obtain an $n + 1$ burn solution with a longer transfer time.

For the solutions, the new coast arc was extended so that a nonoptimal burn arc was present in the guess. This new burn made the guess violate boundary conditions but it aided in the convergence of iterations.

There are three options for creating the next transfer in the family: extend the transfer to the right, extend it to the left, or extend it in both directions. However, because of convergence difficulties, this last option is not favored. Consider extension to the right. In this family of solutions, the extension corresponds to adding the new burn closer to the final orbit. The resulting transfer is represented by point 6 in Fig. 5. Here the new burn has zero length. Starting with point 6, solutions with longer transfer times were easily found, but solutions with shorter transfer times were not found at all.

Now consider the second option, extension to the left. Physically, this extension corresponds to adding a burn near the initial orbit. The resulting transfer is represented by point 3 in Fig. 5. Here the new burn has zero length. Extreme numerical difficulty was discovered in attempting to find a solution with a greater transfer time than point 3; however, solutions with lower transfer times were found constituting branch 3–4–5. Additionally, note that this branch, though a branch of optimal solutions, is unfavorable when compared to branch 6–7 of the family. This example of multiplicity may be viewed as a rearrangement of the burns in the trajectory. It has not been shown analytically, but there is likely a connection to a similar result for nonoptimal impulsive trajectories.[14]

By the preceding discussion, points 2, 3, and 6 are, in fact, equivalent transfers. The only difference between these transfers is the addition of a coast arc, which makes no difference in the cost associated with the transfer. This equivalence means that the branches of the family are connected, and these connections are as follows, with the transfer time increasing: 1 to 2 (which is equivalent to 6) to 7, or 5 to 4 to 3 (which is equivalent to 2).

Note, too, that the transfers represented by points 2, 3, 4, 6, and 7 are optimized with respect to transfer time. It may sound peculiar for more than one solution on the same branch to be time optimal; however, the shorter time-optimal solution has fewer burns, for example, both points 2 and 6 are equivalent two-burn solutions. The Hamiltonian increases as the one traverses the 6–7 branch, then decreases again to zero as one arrives at point 7. Likewise, the Hamiltonian decreases to zero as one traverses the branch from point 5 to point 4, then increases and decreases to zero again as one tranverses the branch from point 4 to point 3.

Figure 7 shows the switching function corresponding to the transfer represented by point 7. Compare this to Fig. 6. The situation has repeated itself; the terminal switching points in Fig. 7 are zero. Clearly, one may attempt to expand this family of transfers from point 7.

Evidence of the existence of multiple solutions was found. For a specified problem (including specification of the transfer time and the number of burns), there may exist more than one extremal transfer. Such multiple solutions are represented by any point on branch 3–4 and any point on branch 6–7, which have equal transfer times, roughly between 27 and 33. Conditions for multiplicity are not clear, but it is clear that solutions are not necessarily unique. It is also clear that one cannot say that just because the transfer time for one solution is longer than another, the former has a greater final mass.

One cannot help but wonder why the solutions of branch 6–7 are more fuel conservative than those of branch 3–4. Both branches are extensions of branch 1–2, but the difference is where the new burn is placed. When the burn is placed near the initial orbit, far from the attracting body, the branch is unfavorable. When the burn is placed near the final orbit, close to the attracting body, the branch is

favorable. A principle often seen in impulsive trajectories appears to carry over in some form to finite burn trajectories; it appears to be better to implement changes in velocity near the attracting body, where changes in velocity will produce large increases in the already large kinetic energy, as opposed to far away from the attracting body, where kinetic energy is lower.

Extremals About an Oblate Planet Without Drag

In this section, another example transfer is presented. However, this time it is a three-burn transfer whose terminal orbits are more general. The initial orbit has the same semimajor axis and eccentricity as before except now the orbit is inclined 20 deg, has a right ascension of 13 deg, and has an argument of perigee at 15 deg. The final orbit is inclined 1 deg with 0-deg right ascension and an argument of perigee at 0 deg. The product $g_0 I_{sp}$ is 1.313, and the thrust level is 0.03. Again the problem has been nondimensionalized. This solution includes oblateness effects but excludes drag effects, with $J_2 = 1082.61 \times 10^{-6}$. Because it affects the equatorial radius, $r^* = 6578$ km must be specified, but this transfer is free to be scaled by m^*.

The trajectory is shown in Figs. 8 and 9. A plot of the switching function and the angle from the thrust to the velocity vector is shown in Fig. 10. This trajectory is a fixed transfer-time transfer and is similar to a trajectory in branch 6–7 of Fig. 5 with $t_f = 28.75$. Recall that this is a descending trajectory; the initial orbit is higher than the final orbit. For the first burn, $\Delta\upsilon = 0.3616$, $\Delta E = -0.07760$, and $\Delta h = -0.6566$. The burn ends at what would be an orbit of $a = 2.409$, $e = 0.5420$, $\Omega = 8.320$ deg, $\omega = 1.123$ deg, and $I = 1.665$ deg. For the second burn, $\Delta\upsilon = 0.1450$, $\Delta E = -0.1048$, and $\Delta h = -0.1310$. The second burn ends at what would be an orbit of $a = 1.601$, $e = 0.3742$, $\Omega = -1.073$ deg, $\omega = 0.3892$ deg, and $I = 1.202$ deg. For the third burn, $\Delta\upsilon = 0.02420$, $\Delta E = -0.02101$, and $\Delta h = -0.01865$. The final mass for this transfer is 1.1656, the initial mass was 1.527. As a result of the oblateness effects, this transfer has poorer performance than if it could be performed in ideal gravity, where its final mass would be 1.1659.

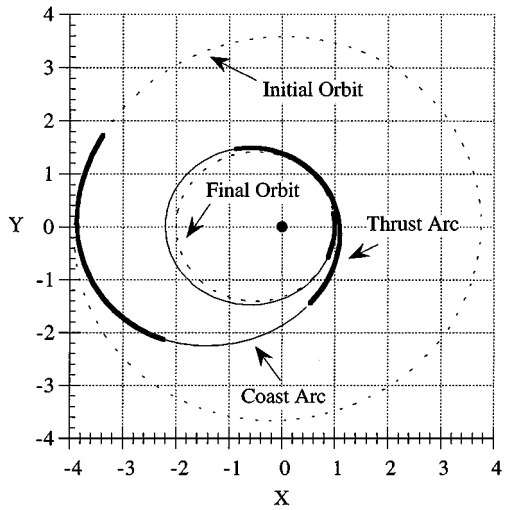

Fig. 8 Projection into *x–y* plane of transfer (nondimensional coordinates).

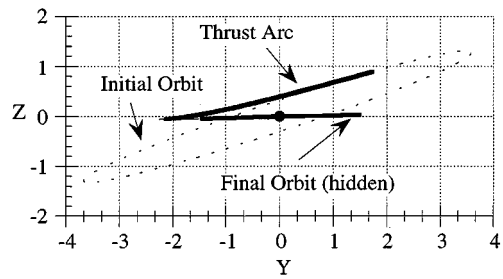

Fig. 9 Projection into *z–y* plane of transfer (nondimensional coordinates).

Table 1 Comparison of three-burn solutions with different dynamic models

t_f	m_f	Drag	Oblateness
29.75	1.1659	No	No
29.75	1.1656	No	Yes
29.75	1.1662	Yes	Yes

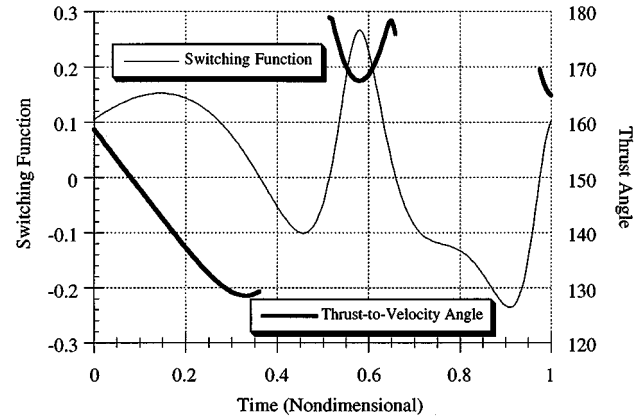

Fig. 10 Thrust-to-velocity angle and switching function for transfer in Figs. 8 and 9.

Note that the change in right ascension was almost exactly divided between the first two burns whereas the change in both inclination and argument of perigee happened almost entirely in the first burn. The change in inclination can be most dramatically seen in Fig. 9. The burn at the top of Fig. 9 is the first burn. The next two burns are difficult to distinguish but not very interesting from this vantage point. The second coasting orbit, or transfer orbit, is quite similar to the final orbit; fittingly, the third burn imparts the least energy of any of the burns.

Extremals About an Oblate Planet with Drag

Having discussed some properties of an extremal transfer about an oblate planet without drag, this discussion can be extended to include drag. In particular, the effect on the final mass will be seen on a particular transfer. This transfer is between terminal orbits identical to those for the transfer shown in Figs. 8 and 9. Table 1 shows the results. If these transfers had much greater transfer times and much greater numbers of burns, the effect would, more than likely, be much greater. The differences discussed here, though small, are best seen in the details of the trajectory.

Comparing the final masses, it turns out that better performance was realized while considering the effects of a retarding force, namely, drag. In fact, this example demonstrates a form of optimal aerobraking. Because the craft descends in the presence of drag, there is no need for thrusting, except to ensure the proper transfer time and the proper orbital elements. In this case, the fuel saved by aerobraking was much greater than that lost due to oblateness effects.

What is the effect on the transversality condition, that is, what is the effect on solutions corresponding to points 2, 3, and 6 in Fig. 5? For ideal gravity, these solutions corresponded to an optimal transfer time. When the drag and oblateness effects were considered, two things were found: an apparently insurmountable difficulty in converging the transversality condition and greater difficulty in hopping from branch to branch of the family. The family discussed earlier has been recovered with oblateness and drag effects; however, the plots are so similar it would be redundant to show them.

The first effect is manifested in the following way: Consider branch 1–2, as the transfer time increases the value of the Hamiltonian decreases. For the ideal gravity case a solution satisfying the transversality condition is easily found. Suppose drag and oblateness terms are added. Now, as the transfer time increases, the Hamiltonian again decreases, but the initial and final values of the switching function are no longer equal. The zero of the switching function no longer indicates a zero of the Hamiltonian because of Theorem 1. Though difficulty in converging the transversality

condition was found, the problem was alleviated by first finding the solution with the switching function zeroed at an appropriate terminal point (initial or final) using the idea from Theorem 1 and then performing a homotopy search for $H = 0$.

The second effect, the difficulty making the connections between branches of the family, is a consequence of Theorem 1 stated earlier and cannot be avoided. Furthermore, the time history of the primer vector will obviously not be periodic on a coast arc that includes drag and oblateness. These effects will, more than likely, not allow some burns to be added in the manner presented earlier. Most likely, this restriction is related to the drag introducing a penalty for long transfers and this will place the global optimal solution at a finite number of burns.

Conclusions

To ease the numerical difficulty of determining a set of optimal solutions, the indirect methods BOUNDSCO and MBCM have been modified with an initial guess searching scheme to solve the orbit transfer mass optimization problem. The scheme combines a new procedure based on a property of the switching function for the optimal control problem, homotopy, and other numerical methods. Numerical solutions of two and three burns are obtained with and without oblateness. These solutions demonstrate effects of drag and oblateness on the optimal transfer.

The presented family gives a set of transfers with identical terminal orbits and parameterized by transfer time. Using this family, we conclude the following for optimal transfers: Transfers between specific orbits for a specific transfer time and a specific number of burns may not be unique, transfers with greater transfer time do not necessarily have greater fuel savings, and these properties persist in the examples even with drag and oblateness effects.

A theorem that applies to optimal orbit transfers has been stated in a general form so that it can be determined whether it applies to other problems. This theorem has been used to point out that in the free transfer-time case, with the terminal points optimized, burn arcs may often be added to solutions. A simple method that utilizes this theorem to add burns to extremal solutions with optimal transfer time has been presented. For this study, every attempt to add burns this way has been successful. Examples are given of solutions that were improved using this method.

Appendix: Proof of Theorem 1

In the usual optimal control formulation, the boundary conditions at t_i and t_f result in the familiar natural boundary conditions on the Lagrange multipliers written as

$$\boldsymbol{\lambda}(t_i) = -\left(\frac{\partial \boldsymbol{\psi}_i}{\partial \boldsymbol{x}}\right)^T \boldsymbol{\nu}_i, \qquad \boldsymbol{\lambda}(t_f) = \left(\frac{\partial \boldsymbol{\psi}_f}{\partial \boldsymbol{x}}\right)^T \boldsymbol{\nu}_f$$

which involve the Lagrange multiplier vectors $\boldsymbol{\nu}_i \in R^{q_1}$ and $\boldsymbol{\nu}_f \in R^{q_2}$. Now, take the dot product of these vectors with vectors called $\boldsymbol{n}_1 \in R^n$ and $\boldsymbol{n}_2 \in R^n$,

$$\boldsymbol{\lambda}(t_i)^T \boldsymbol{n}_1 = -\boldsymbol{\nu}_i^T \left(\frac{\partial \boldsymbol{\psi}_i}{\partial \boldsymbol{x}}\right) \boldsymbol{n}_1, \qquad \boldsymbol{\lambda}(t_f)^T \boldsymbol{n}_2 = -\boldsymbol{\nu}_f^T \left(\frac{\partial \boldsymbol{\psi}_f}{\partial \boldsymbol{x}}\right) \boldsymbol{n}_2$$

This shows that, at both the initial and final times, any vector in the null space of the relevant constraint gradient matrix is perpendicular to the respective Lagrange multiplier vector. Assumption 2 of Theorem 1 indicates appropriate choices for $\boldsymbol{n}_1$ and $\boldsymbol{n}_2$ as

$$\boldsymbol{n}_1 = \boldsymbol{f}[\boldsymbol{x}(t_i), t_i], \qquad \boldsymbol{n}_2 = \boldsymbol{f}[\boldsymbol{x}(t_f), t_f]$$

With these choices, the Hamiltonian at either terminal time may be written in the following form:

$$H(\boldsymbol{x}, \boldsymbol{w}, u, \boldsymbol{\lambda}) = [\boldsymbol{\lambda}^T \boldsymbol{g}(\boldsymbol{x}, \boldsymbol{w}, t) + M(\boldsymbol{x}, t)]u + L(\boldsymbol{x}, t)$$

Statements (1) and (2) follow immediately. QED

Acknowledgment

This work was sponsored by NASA under Contract NAG8-921.

References

[1]Lawden, D. F., *Optimal Trajectories for Space Navigation*, Butterworths, London, 1963.

[2]Enright, P. J., and Conway, B. A., "Optimal Finite-Thrust Spacecraft Trajectories Using Collocation and Nonlinear Programming," *Journal of Guidance, Control, and Dynamics*, Vol. 14, No. 5, 1991, pp. 981–985.

[3]Enright, P. J., and Conway, B. A., "Discrete Approximations to Optimal Trajectories Using Direct Transcription and Nonlinear Programming," *Journal of Guidance, Control, and Dynamics*, Vol. 15, No. 4, 1992, pp. 994–1002.

[4]Zondervan, K. P., Lincoln, L. J., and Caughey, T. K., "Optimal Low-Thrust, Three-Burn Orbit Transfers with Large Plane Changes," *Journal of the Astronautical Sciences*, Vol. 32, No. 3, 1984, pp. 407–427.

[5]Vulpetti, G., and Montreali, R. M., "High-Thrust and Low-Thrust Two-Stage LEO-LEO Transfer," *Acta Astronautica*, Vol. 15, No. 12, 1987, pp. 973–979.

[6]Redding, D. C., "Optimal Low-Thrust Transfers to Geosynchronous Orbit," NASA John H. Glenn Research Center at Lewis Field, SUDAAR 539, Cleveland, OH, Sept. 1983.

[7]McAdoo, S., Jr., Jezewski, D. J., and Dawkins, G. S., "Development of a Method for Optimal Maneuver Analysis of Complex Space Missions," NASA TN D-7882, April 1975.

[8]Horsewood, J. L., Suskin, M. A., and Pines, S., "Moon Trajectory Computational Capability Development," NASA John H. Glenn Research Center at Lewis Field, TR-90-51, Cleveland, OH, July 1990.

[9]Edelbaum, T. N., Sackett, L. L., and Malchow, H. L., "Optimal Low Thrust Geocentric Transfer," AIAA Paper 73-1074, Nov. 1973.

[10]Brown, K. R., Harrold, E. F., and Johnson, G. W., "Rapid Optimization of Multiple-Burn Rocket Flights," NASA CR-1430, Sept. 1969.

[11]Oberle, H. J., "BOUNDSCO—Hinweise zur Benutzung des Mehrzielverfahrens für die numerische Lösung von Randwerproblemen mit Schaltbedingungen," *Hamburger Beiträge zur Angewandten Mathematik*, Berichte 6, 1987.

[12]Chuang, C.-H., and Speyer, J. L., "Periodic Optimal Hypersonic SCRAM Jet Cruise," *Optimal Control Applications and Methods*, Vol. 8, 1987, pp. 231–242.

[13]Chobotov, V. A. (ed.), *Orbital Mechanics*, AIAA, Washington, DC, 1991, p. 116.

[14]Lion, P. M., and Handelsman, M., "Primer Vector on Fixed-Time Impulsive Trajectories," *AIAA Journal*, Vol. 6, No. 1, 1968, pp. 127–132.

[15]Anderson, J. D., *Introduction to Flight*, McGraw–Hill, New York, 1989, pp. 74–79.

[16]Space Technology Labs., *Flight Performance Handbook for Orbital Operations*, Wiley, New York, 1963, pp. 222–224.

[17]Bryson, A. E., and Ho, Y.-C., *Applied Optimal Control*, Hemisphere, New York, 1989, pp. 42–50, 110–117.

[18]U.S. Committee on Extension to the Standard Atmosphere (COESA), *U.S. Standard Atmosphere, 1976*, Government Printing Office, Washington, DC, 1976, pp. 50–73.

[19]Lawden, D. F., "Fundamentals of Space Navigation," *Journal of the British Interplanetary Society*, Vol. 13, No. 2, 1954, pp. 87–101.

F. H. Lutze Jr.
Associate Editor